

Numerical solution of nonlinear Schrödinger equation by a hybrid pseudospectral-variational quantum algorithm

Nikolas Köcher,¹ Hendrik Rose,² Jörg Schumacher,^{3,4} and Stefan Schumacher^{1,2,5}

¹*Department of Physics and Center for Optoelectronics and Photonics Paderborn (CeOPP), Paderborn University, D-33098 Paderborn, Germany*

²*Institute for Photonic Quantum Systems (PhoQS),*

Paderborn University, D-33098 Paderborn, Germany

³*Institute of Thermodynamics and Fluid Mechanics,*

Technische Universität Ilmenau, D-98684 Ilmenau, Germany

⁴*Tandon School of Engineering, New York University, New York City, NY 11201, USA*

⁵*Wyant College of Optical Sciences, University of Arizona, Tucson, AZ 85721, USA*

(Dated: July 4, 2024)

The time-dependent one-dimensional nonlinear Schrödinger equation (NLSE) is solved numerically by a hybrid pseudospectral-variational quantum algorithm that connects a pseudospectral step for the Hamiltonian term with a variational step for the nonlinear term. The Hamiltonian term is treated as an integrating factor by forward and backward Fourier transformations, which are here carried out classically. This split allows us to avoid higher-order time integration schemes, to apply a first-order explicit time stepping for the remaining nonlinear NLSE term in a variational algorithm block, and thus to avoid numerical instabilities. We demonstrate that the analytical solution is reproduced with a small root mean square error for a long time interval over which a nonlinear soliton propagates significantly forward in space while keeping its shape. We analyze the accuracy of the quantum algorithm and compare it with classical approaches. Furthermore, we investigate the influence of algorithm parameters on the accuracy of the results, including the temporal step width and the depth of the quantum circuit.

I. INTRODUCTION

The question on the application of quantum computing methods for the solution of linear and nonlinear ordinary or partial differential equations has received substantial interest in the past years [1–4]. It is yet an open point if the specific and unique properties of quantum algorithms in comparison to classical ones lead to faster and more efficient numerical solution methods leaving aside the technological hurdles of present noisy intermediate scale quantum (NISQ) devices [5]. This comprises their encoding capabilities, which grow exponentially with the qubit number, and the unique parallelism and correlations due to the entanglement of multiple qubits. The question has been approached from different methodological directions and problem tasks. Fundamental nonlinear partial differential equations such as the nonlinear Schrödinger or Burgers equations appear in many applications ranging from nonlinear optics [6, 7], Bose-Einstein condensation [8], oceanography [9] via fluid turbulence [10] to astrophysical jets [11]. Solution algorithms comprise (i) a combination of quantum linear systems algorithms (QLSA) with homotopy perturbation methods [12], (ii) linearization of nonlinear problems [13, 14] by Carleman embedding [15], (iii) quantum feature map encodings of nonlinearities [16] as in kernel methods of machine learning [17], and (iv) variational quantum algorithms (VQA) [18–20]. VQA are inspired by variational quantum eigenvalue solvers which search a ground state of a many-particle quantum system by minimization of an energy functional [21]. The class of variational methods provides the motivation for the present study.

Here, we present a numerical solution method of the one-dimensional nonlinear Schrödinger equation (NLSE) which applies a pseudospectral-variational quantum algorithm. This algorithm combines a pseudospectral split-step method for the linear part of the NLSE and a variational algorithm for the nonlinear part. Variational algorithms typically rely on low-order schemes for the time-advancement [18, 22]. In case of the NLSE this causes numerical instabilities such that higher-order time stepping methods have to be applied classically. The present split method overcomes this stability problem. We investigate the dependence of the results on the degree of entanglement of the parametric quantum circuit. This degree of entanglement depends on the depth of the quantum circuit which is the dependence to be investigated. It is shown that the algorithm can solve the equation for a longer period of at least up to 100 integration time steps, which is an exceptionally long integration period for a quantum algorithm. Figure 1 shows an illustrative simulation result obtained with the algorithm presented in the present paper.

Variational quantum algorithms – hybrid quantum-classical algorithms – have been used to solve linear and nonlinear partial differential equations in the past years. This includes linear one-dimensional advection-diffusion equations for simple transport problems [22–25] and heat equations in one and two dimensions [26, 27]. Nonlinear problems include the steady one-dimensional NLSE [18] and the one-dimensional Burgers equation for the nonlinear steepening of a sine wave [18, 20, 28]. In refs. [20, 28] an alternative Feynman-Kitaev algorithm is used which orders spatial and temporal qubits in one register and

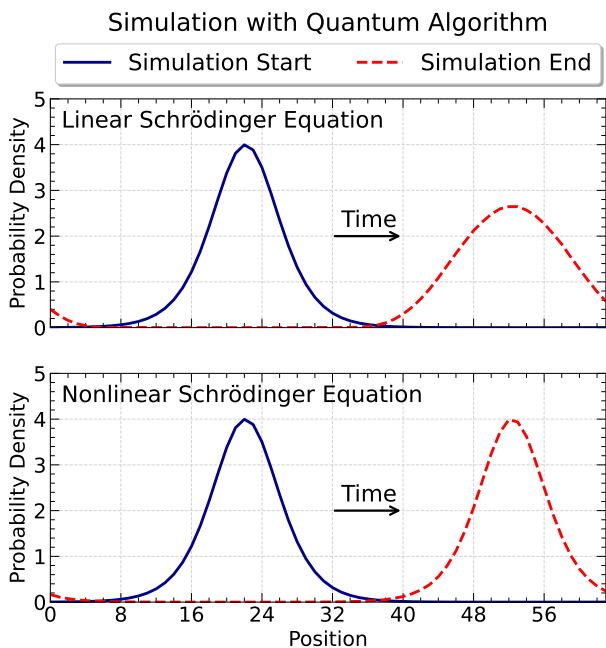


FIG. 1. Illustrative simulation result obtained with the quantum algorithm presented in this paper. Top: time evolution of a wave packet in the linear Schrödinger equation; the quadratic dispersion leads to broadening with increasing propagation distance. Bottom: time evolution of a bright soliton in the nonlinear Schrödinger equation; the initial wave packet maintains its shape. More details are provided in Sec. II.

thus avoids the time stepping. However, this enhances the number of qubits in the required quantum register and thus limits an application for current NISQ devices to a few time steps only.

The outline of this manuscript is as follows. In Sec. II we summarize the NLSE and analytical solutions for the validation of the method together with the basic ideas of variational algorithms and the split-step method. This includes the implementation of the nonlinear term $s|\Psi|^2\Psi$ (see Sec. II A) and the evaluation of the cost function. The numerical results obtained from the quantum algorithm are presented in Sec. III, where we also analyze the accuracy of the method compared to classical algorithms and investigate the dependence on algorithm parameters. We conclude with a summary and outlook in Sec. IV.

II. METHODS

A. Nonlinear Schrödinger Equation

The one-dimensional, time-dependent nonlinear Schrödinger equation (NLSE), which is also known as the Gross-Pitaevskii equation in the context of Bose-Einstein condensation, for the complex wave function

$\Psi(x, t)$ is given in dimensionless form by

$$i\frac{\partial\Psi}{\partial t} = -\frac{1}{2}\frac{\partial^2\Psi}{\partial x^2} + V\Psi - s|\Psi|^2\Psi, \quad \Psi(x, 0) = \Psi_0(x), \quad (1)$$

where the nonlinear coupling constant s describes the strength of the nonlinearity. The potential energy operator is V . The case $s > 0$ gives rise to a focusing nonlinearity and bright soliton solutions; the case $s < 0$ leads to defocusing nonlinearities and dark solitons. The NLSE is integrable in one dimension. For the case of $V = 0$, there exist several analytical solutions of (1). For $x \in \mathbb{R}$, $s = 1$, and the initial condition

$$\Psi_0(x) = a \operatorname{sech}(a(x - x_0))e^{iv(x - x_0)}, \quad (2)$$

one gets the following analytical solution

$$\Psi(x, t) = a \operatorname{sech}(a(x - x_0 - vt))e^{iv(x - x_0) + \frac{i}{2}(a^2 - v^2)t}, \quad (3)$$

with constants $a > 0$, $v > 0$, and $x_0 \in \mathbb{R}$. For $s = 1$ this solution corresponds to soliton propagation.

We can furthermore construct a solution $\Psi_p(x, t)$ that satisfies periodic boundary conditions on a finite domain of length L

$$\Psi_p(x, t) = \max(\{\Psi(x + kL) | k \in \mathbb{Z}\}). \quad (4)$$

This analytical solution will be used as the test case for the present algorithm. Throughout the rest of the manuscript $V = 0$.

B. Variational Quantum Algorithms

VQAs are hybrid quantum-classical algorithms where a parameterized cost function C is minimized by an optimizer [3]. The cost function is evaluated by a quantum circuit which is composed of n qubits and single- and two-qubit gates, the cost minimum search is performed classically in an N -dimensional parameter space that contains a parameter vector $\boldsymbol{\lambda}$. This parameter vector $\boldsymbol{\lambda}$, which consists of the angles of the single-qubit unitary rotation gates $\boldsymbol{\lambda} = (\lambda_1, \lambda_2, \dots, \lambda_N) \in \mathbb{R}^N$, is the input to the algorithm. For each time step, the trial solutions for the NLSE $|\Psi(t + \Delta t)\rangle$, represented by normalized quantum states $|\psi(t + \Delta t)\rangle$ are generated by the parametric quantum circuit

$$|\psi(\boldsymbol{\lambda})\rangle = U(\boldsymbol{\lambda})|0\rangle^{\otimes n}. \quad (5)$$

Because the normalization of $|\Psi(t)\rangle$ and $|\psi(t)\rangle$ differs, they are related by a constant factor as further explained in section II D. The cost function $C(\boldsymbol{\lambda})$ is then also evaluated on the quantum device in a Hadamard test-like circuit [18, 22]. This implies to determine the following overlap

$$\begin{aligned} C(\boldsymbol{\lambda}) &= \|\psi(\boldsymbol{\lambda}) - F[|\psi(t)\rangle]\|_2^2 \\ &= |\langle\psi(\boldsymbol{\lambda})|F[|\psi(t)\rangle]\rangle|^2 \rightarrow \min, \end{aligned} \quad (6)$$

where $F[|\psi(t)\rangle]$ is the (nonlinear) iteration from the past step t in correspondence with the underlying partial differential equation (PDE). Note, that we dropped the additional constant terms in the cost function. Discretized in space and time, Eq. (1) can be formally written as

$$\psi(x_j, t + \Delta t) = F[\psi(x_k, t)], \quad (7)$$

see also next subsection. Multiple repeated measurements of identically prepared quantum states per iteration step evaluate the costs. These costs are minimized with a limited-memory Broyden-Fletcher-Goldfarb-Shanno algorithm with constant lower and upper bounds for λ_k (L-BFGS-B) which applies a quasi-Newton method for solving unconstrained, nonlinear optimization problems [29]. Thereby, the Hessian matrix of the cost function is approximated by the evaluation of the gradients (or the approximated gradients) in order to find the descent direction in the hyperparameter landscape. The optimal parameter set λ^* initializes the ansatz function such that the solution of the given problem can be observed [3]. We use random initial parameters for the first time step and the optimized parameters from the previous step for all subsequent steps.

C. Pseudospectral Split-Step Method

We consider the solution on a finite domain $x \in [-\pi, \pi)$ and discretize the interval with M grid points $x_j = -\pi + 2\pi j/M$ ($0 \leq j < M$). We use periodic boundary conditions such that $x_M \equiv x_0$. The temporal evolution will be solved on an equidistant time grid starting from $t_0 = 0$ and a fixed timestep width of Δt . We apply operator splitting to treat the linear and nonlinear operators in the NLSE (1) separately in a two-step process [30, 31]. First, we compute an implicit substep for the linear Laplacian operator using the exact solution in Fourier space, which implicitly includes the periodic boundary condition. The wavenumbers of the Fourier modes are given by $k_j = j - M/2$. Then, we compute an explicit step for the nonlinear operator by using an Euler step. The time-discretized stepping scheme from t to $t + \Delta t$ proceeds in two substeps. The first implicit substep is given by

$$\tilde{\Psi}(x_j, t) = \mathcal{F}^{-1} \left(\exp \left(-\frac{i}{2} k_j^2 \Delta t \right) \mathcal{F}(\Psi(x_j, t)) \right). \quad (8)$$

In case of $V \neq 0$, we could treat the additional potential term of the NLSE again with an integrating factor $\exp(-iV\Delta t)$ [32]. Subsequently, the second explicit (Euler) substep follows to

$$\Psi(x_j, t + \Delta t) = \tilde{\Psi}(x_j, t) + is\Delta t |\tilde{\Psi}(x_j, t)|^2 \tilde{\Psi}(x_j, t). \quad (9)$$

The symbols \mathcal{F} and \mathcal{F}^{-1} stand for the discrete Fourier and inverse Fourier transforms, respectively.

Using the split-step method has a central advantage over other methods in that it remains stable for long

temporal step widths Δt due to the absence of the second derivative in x . This is important considering the limited number of time steps that can be done with a VQA, partially owed to the accumulating errors of the optimization. An explicit stepping scheme would not be applicable to solve the NLSE by VQA with the same amount of resources, since it requires a smaller Δt while the total amount of accurate VQA steps remains fixed. Furthermore, all required steps can be mapped to a quantum circuit.

Next, we will discuss the realization of this scheme with a quantum algorithm. Note that the implicit step Eq. (8) requires two Fourier transforms and a multiplication with a phase. The latter can be done with a circuit shown in Ref. [32], while the former is realized by a straightforward application of the quantum Fourier transform algorithm [33, 34]. The explicit step can be computed by VQA.

D. Evaluation of the Cost Function

We expand the wave function into the n -qubit basis as follows

$$|\Psi(t)\rangle = \sqrt{\frac{2a}{\Delta x}} \sum_{j=0}^{2^n-1} \psi(x_j, t) |j\rangle = \sqrt{\frac{2a}{\Delta x}} |\psi(t)\rangle, \quad (10)$$

where $|j\rangle$ denotes the n -qubit basis state corresponding to the binary representation of j . Consequently, $M = 2^n$ with a qubit number n . Equation (10) provides a construction for switching between the representations and satisfies the normalization constraint

$$\langle \psi(t) | \psi(t) \rangle = 1. \quad (11)$$

Since the wave function is normalized according to

$$\int_{-\infty}^{\infty} |\Psi(x, t)| dx = 2a, \quad (12)$$

we do not need an extra optimization parameter for the amplitude. The computed solution is related to the solution of the NLSE by a constant factor. Note that the initial condition for the soliton at $t = 0$ is directly implemented into the cost function.

We formulate a cost function for the operator F that describes the explicit step Eq. (9). F is diagonal and its elements $f_{j,j}$ have the form:

$$f_{j,j} = 1 + is\Delta t \frac{2a}{\Delta x} |\psi(x_j, t)|^2. \quad (13)$$

Note that the factor $2a/\Delta x$ originates from the normalization conditions Eqs. (11) and (12).

Substituting F into Eq. (6) and omitting constant terms yields the following cost function

$$C(\lambda_{t+\Delta t}) = s\Delta t \frac{2a}{\Delta x} \text{Im} \left\{ \langle \psi(t + \Delta t) | \tilde{\psi}(t) \tilde{\psi}^*(t) | \tilde{\psi}(t) \rangle \right\} - \text{Re} \left\{ \langle \psi(t + \Delta t) | \tilde{\psi}(t) \rangle \right\}, \quad (14)$$

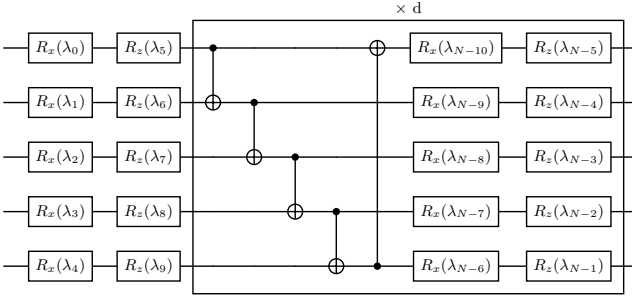


FIG. 2. Ansatz circuit for $n = 5$ qubits. The depth d determines the number of layers of controlled NOT (CNOT) gates, each followed by single qubit rotations R_x and R_z that are applied after an initial layer of rotation gates.

where $|\tilde{\psi}(t)\rangle$ is the state vector after the implicit substep and $|\psi(t + \Delta t)\rangle$ is a function of $\boldsymbol{\lambda}_{t+\Delta t}$.

To initialize the state $|\psi(t)\rangle = U(\boldsymbol{\lambda}_t)|0\rangle^{\otimes n}$ and the trial state $|\psi(t + \Delta t)\rangle = U(\boldsymbol{\lambda}_{t+\Delta t})|0\rangle^{\otimes n}$ we use the parameterized ansatz circuit shown in Fig. 2 consisting of multiple layers of single-qubit rotations and controlled NOT gates, where we define the depth d of the quantum circuit as the number of layers of controlled NOT (CNOT) gates, each followed by a layer of single qubit rotation gates R_x and R_z , that are applied after the initial layer of rotation gates. Note that we tested other ansatz circuits as well, however, the one presented here was the most accurate one. For each time step, the state $|\tilde{\psi}(t)\rangle$ after the first substep is then obtained by additionally applying the quantum Fourier transform (QFT) [33], multiplying by the appropriate phase for each k in Fourier space, see Eq. (8), and applying the inverse QFT. This includes

$$|\tilde{\psi}(t)\rangle = \tilde{U}(\boldsymbol{\lambda}_t)|0\rangle^{\otimes n}, \quad (15)$$

with

$$\tilde{U}(\boldsymbol{\lambda}_t) = (\text{QFT})^\dagger X^{(n-1)} U_{\text{ph}} X^{(n-1)} (\text{QFT}) U(\boldsymbol{\lambda}_t). \quad (16)$$

After applying the QFT, the zero frequency component of the state is shifted to the center of Fourier space by applying an X gate to the most significant qubit and another X gate before the inverse QFT reverses this shift. Following reference [32], U_{ph} can be constructed using n^2 phase and controlled phase gates

$$U_{\text{ph}} = \prod_{i,j=0}^{n-1} P_{ij} \quad (17)$$

with

$$P_{ij} = \begin{cases} P^{(i)}(\gamma(2^{2i} - 2^{n+i})) & \text{if } i = j \\ CP^{(ij)}(\gamma 2^{i+j}) & \text{if } i \neq j \end{cases} \quad (18)$$

where $\gamma = -\Delta t/2$ and P and CP denote the phase and controlled phase gate.

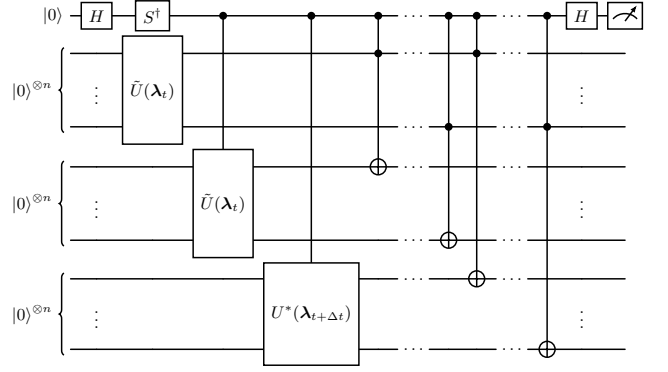


FIG. 3. Circuit for computing the nonlinear term in the cost function. Its value is obtained via a computational basis measurement of the ancilla qubit.

Using these circuits the second term in Eq. (14) can be computed using a Hadamard test, see e.g. Ref. [22] for a detailed description. Figure 3 shows the circuit used to evaluate the nonlinearity, denoted as the quantum nonlinear processing unit (QNPU),

$$\text{Im} \left\{ \sum_{j=0}^{2^n-1} \psi_j(t + \Delta t) |\tilde{\psi}_j(t)|^2 \tilde{\psi}_j(t) \right\}. \quad (19)$$

The QNPU is based on the circuits from refs. [18, 19] for evaluating functions of the form

$$F = f^{(1)*} \prod_{j=1}^r f^{(j)}. \quad (20)$$

To arrive at the circuit shown here we use $r = 3$, $f^{(1)} = f^{(2)} = \tilde{\psi}(t)$ and $f^{(3)} = \psi^*(t + \Delta t)$ and add an S^\dagger -gate to compute the imaginary part instead of the real part of the expression. The value of expression (19) is then obtained as the expectation value of a Z -measurement performed on the ancilla (first) qubit. The unitary $U^*(\boldsymbol{\lambda}_{t+\Delta t})$ initializes the complex conjugate of the state $|\psi(t + \Delta t)\rangle$ and is obtained by applying $U(\boldsymbol{\lambda}_{t+\Delta t})$ but changing the sign of the angles of rotation of the R_x and R_z gates.

To keep the simulation times in a reasonable limit, we do not evaluate the cost function on a simulated quantum circuit for subsequent simulations. Nevertheless, we verified that simulated quantum circuits yield the same value for the cost function compared to matrix multiplication. For the same reason, we compute the Fourier transform classically with a fast Fourier transform (FFT) algorithm rather than with the QFT algorithm. The quantum circuit for the VQA is implemented with Qiskit quantum simulation software [35]. The classical optimization of the quantum circuit is done with the Qiskit implementation of the L-BFGS-B optimizer algorithm. A relevant parameter for the optimization algorithm is `ftol` which is an upper bound for the relative error of two consecutive iteration steps that must be fulfilled for the optimization to terminate.

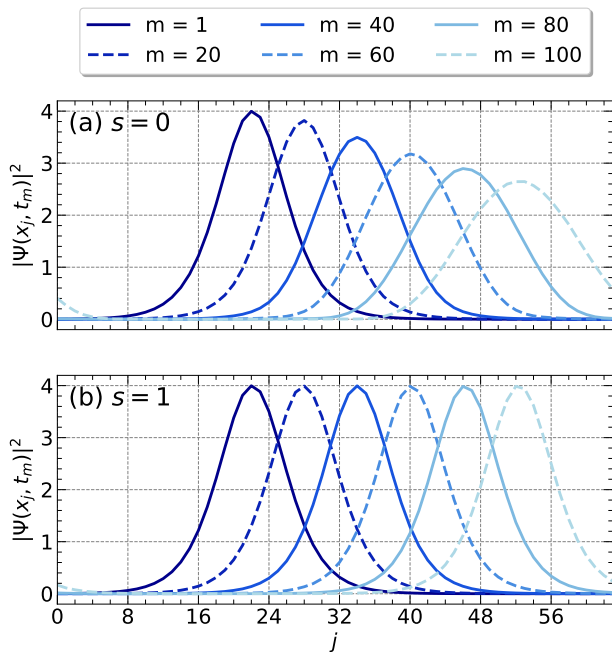


FIG. 4. Simulation results obtained from the quantum algorithm introduced in Sec. II are shown for selected time steps t_m for (a) the linear Schrödinger equation $s = 0$ and (b) the NLSE for $s = 1$. The results are obtained for a qubit number of $n = 6$ with the statevector simulator. The discrete output time steps are denoted as m in the legend. Line styles given are for both panels.

Qiskit can be used in three different ways, (1) as an ideal simulator without quantum circuit noise monitoring the complex quantum statevector (statevector simulator), (2) as an ideal simulator without quantum circuit noise and with measurement noise (qasm simulator), and (3) as a simulator that emulates the NISQ devices with quantum circuit and measurement noise. We will only use (1) throughout this work.

III. RESULTS

This section is divided into two parts. First, we will demonstrate simulation results with the presented algorithm and will discuss its suitability and accuracy. Secondly, we will investigate the importance of algorithm parameters, i.e., the width of the timestep and the depth of the quantum circuit.

A. Simulation Results and Accuracy Analysis

Henceforth, we will use the parameters $a = 2$, $x_0 = -1$, and $v = 10$ for the initial state obtained from $\Psi_p(x, 0)$ in Eq. (4), unless stated otherwise. We apply the quantum algorithm with $n = 6$ qubits, a circuit depth of $d = 12$, a time step of $\Delta t = 3 \cdot 10^{-3}$, and $\text{ftol} = 10^{-14}$ to

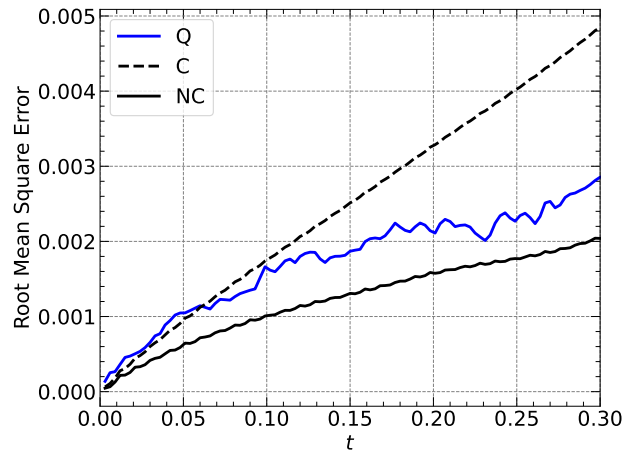


FIG. 5. RMS errors versus time for the simulation shown in Fig. 4(b) together with the RMS error obtained from the classical versions of the algorithm. (Q) stands for quantum, (C) for classical, and (NC) normalized classical; see the text for further details.

compute solutions for the linear case with $s = 0$ and the nonlinear case with $s = 1$, the latter leading to soliton propagation. The simulation results are shown in Fig. 4. Both are obtained for a grid resolution of $M = 64$ and 6 qubits. The simulation demonstrates that our proposed quantum algorithm describes the time evolution correctly over a long propagation range. The analytical solution is visually identical to the numerical solution and therefore not shown to preserve clarity.

The accuracy of the quantum algorithm will be analyzed in the following by comparing the numerical result for the soliton solution with the analytically exact solution given by Eq. (4). For a quantitative analysis we introduce the root mean square error (RMSE), which is given by

$$\text{RMSE}(m) = \sqrt{\frac{1}{2^n} \sum_{j=0}^{2^n-1} ||\Psi_{\text{num}}(x_j, t_m)| - |\Psi_p(x_j, t_m)||^2}, \quad (21)$$

where Ψ_{num} denotes the numerical result.

To make a more insightful comparison, we do not only investigate the quantum algorithm (Q), but also the classical version of it (C), as well as the classical version where we manually normalize the solution after each time step (NC), where classical version means that we use the classical algorithm given by Eqs. (8) and (9). The respective RMSE will be referred to as Q-RMSE, C-RMSE, and NC-RMSE. Figure 5 shows all three error measures versus time t for the same parameters as in Fig. 4. We see that all errors are on the same order of magnitude. The Q-RMSE is smaller than the C-RMSE for most times t , which comes from the intrinsic norm conservation in quantum algorithms, which the classical algorithm lacks.

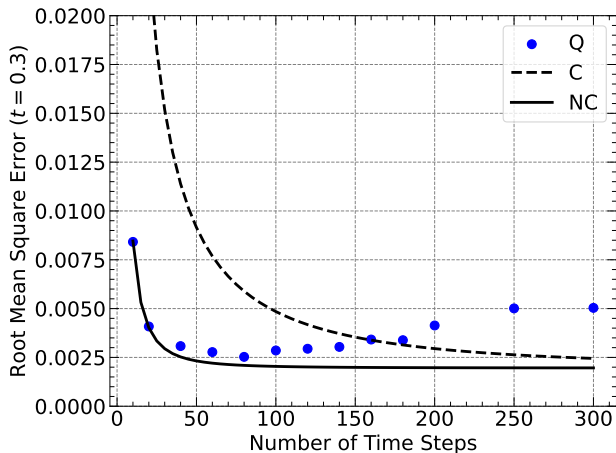


FIG. 6. RMS error for a VQA simulation with the same parameters as the simulation shown in Fig. 4(b), but with different numbers of time steps used to span an interval of $t = 0.3$ time units. Only the RMS error at $t = 0.3$ is shown and is compared with the classical version of the algorithm with and without normalizing the state after every time step. The legend is the same as in Fig. 5.

This becomes clear when comparing the Q-RMSE against the NC-RMSE, where we note that the NC-RMSE is a lower bound for the Q-RMSE. Note that due to the random initial conditions before the optimization, the Q-RMSE will depend on the random numbers, but the general trend remains the same. Further simulations show that larger values for ftol are sufficient, more precisely, a value of $\text{ftol} = 10^{-9}$ is sufficient to obtain a Q-RMSE smaller than the C-RMSE for most times.

B. Dependence on Algorithm Parameters

In this section we analyze the impact of parameters, including the timestep width Δt and the quantum circuit depth, on the accuracy of the numerical results.

We start by analyzing the dependence on Δt . Figure 6 shows the Q-RMSE for the last simulated time step at $t = 0.3$ for multiple VQA runs, that only differ by the chosen temporal step width Δt and thus, in the number of simulated time steps, which are plotted on the x -axis. Fig. 6 also depicts the C-RMSE and the NC-RMSE. We observe that the Q-RMSE and the NC-RMSE are similar for a wide range of time steps while the latter is always smaller, which is compatible with the result from Sec. III A. For larger numbers of time steps, however, the Q-RMSE exceeds both, the NC-RMSE and the C-RMSE due to the accumulated errors in the classical optimization. For small numbers of time steps, all algorithms produce large RMSE because the algorithms become unstable for large Δt . In conclusion, one can identify a global minimum at which the Q-RMSE is minimized, which corresponds to 80 steps for the fixed integration

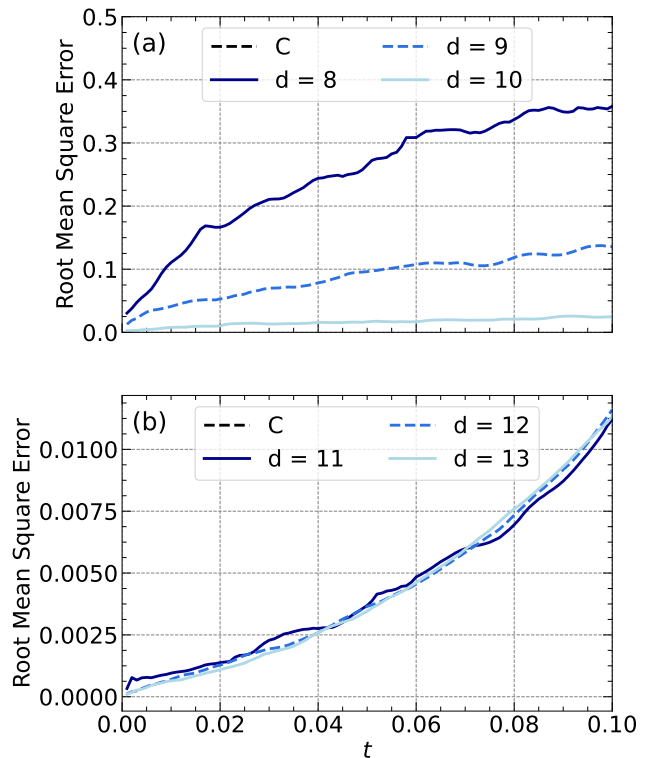


FIG. 7. The RMS is shown for the classical version of the quantum algorithm and for the quantum algorithm with different circuit depths of (a) $d = 8, 9$, and 10 (b) $d = 11, 12$, and 13.

time interval of $t = 0.3$.

Finally, we will discuss the dependence of the Q-RMSE on the circuit depth d . The quantum circuit has $2n(d+1)$ free parameters, while the state in Eq. (10) has 2^{n+1} unknowns, which means that for $n = 6$, we have more free parameters than unknowns if $d \geq 10$, i.e., the optimization is overdetermined and underdetermined otherwise. Figure 7 shows the Q-RMSE error for 6 VQA runs using $\Delta t = 10^{-3}$, $x_0 = 0$, and $\text{ftol} = 10^{-13}$ together with the respective C-RMSE. The simulations differ only in the depth d of the quantum circuit. We see that the error converges for a depth of $d' = 11$, as deeper circuits do not reduce the error significantly. This behavior is expected, since the optimization is overdetermined for $d \geq d'$. In contrast, the Q-RMSE for $d < 10$ is large, since the optimization is underdetermined. Overparametrizations have been discussed for quantum neural networks recently [36]. In that case, the authors could derive an upper bound on the number of network parameters by means of the dimension of the Lie algebra, the latter of which is formed by the infinitesimal generators of the network unitary.

IV. CONCLUSION

In this work, we introduce a quantum algorithm that combines VQA and pseudospectral split-step methods and demonstrate its suitability for solving the NLSE for sufficiently deep quantum circuits for a longer time period in which a soliton solution propagates over a significant distance in space. The split-step method allowed us to keep a first-order time integration scheme for the nonlinear terms of the NLSE while treating the linear part as an integrating factor in combination with Fourier transforms. This keeps the quantum circuit implementation feasible and allowed us to run the algorithm for longer time intervals than typically seen.

The main bottleneck in the presented algorithm is the classical optimization that is required for the VQA. It not only restrains the scalability for larger systems with more qubits by requiring a high-dimensional classical optimization, but also must remain accurate, which constitutes another challenge. One promising candidate for an efficient optimization is surrogate-based optimization [37]. Besides these open problems, our results demonstrate that the algorithm works and generates accurate results.

The present work should be considered as a proof-of-concept study. A continuation of the study along these lines should imply a number of steps: (1) an inclusion of the Fourier transformations in the form of quantum Fourier transformations into the algorithms, (2) a switch from an ideal statevector simulation to quantum simulation with measurement noise, and eventually (3) an implementation on a NISQ device. These steps will be reported elsewhere.

ACKNOWLEDGMENTS

The authors gratefully acknowledge the computing time made available to them on the high-performance computer Noctua 2 at the NHR Center Paderborn Center for Parallel Computing (PC²). This center is jointly supported by the Federal Ministry of Education and Research and the state governments participating in the NHR (www.nhr-verein.de/unsere-partner). The work of JS is supported by the European Union (ERC, Meso-Comp, 101052786). Views and opinions expressed are however those of the author only and do not necessarily reflect those of the European Union or the European Research Council. Neither the European Union nor the granting authority can be held responsible for them.

-
- [1] A. Montanaro, Quantum algorithms: An overview, *npj Quantum Information* **2**, 15023 (2016).
 - [2] I. H. Deutsch, Harnessing the power of the second quantum revolution, *PRX Quantum* **1**, 020101 (2020).
 - [3] M. Cerezo, A. Arrasmith, R. Babbush, S. C. Benjamin, S. Endo, K. Fujii, J. R. McClean, K. Mitarai, X. Yuan, L. Cincio, and P. J. Coles, Variational quantum algorithms, *Nature Reviews Physics* **3**, 625 (2021).
 - [4] S. Succi, W. Itani, K. R. Sreenivasan, and R. Steijl, Quantum computing for fluids: Where do we stand?, *Europhysics Letters* **144**, 10001 (2023).
 - [5] J. Preskill, Quantum computing in the NISQ era and beyond, *Quantum* **2**, 79 (2018).
 - [6] G. Fibich, *The nonlinear Schrödinger equation* (Springer, 2015).
 - [7] C. Lüders, M. Pukrop, F. Barkhausen, E. Rozas, C. Schneider, S. Höfling, J. Sperling, S. Schumacher, and M. Aßmann, Tracking quantum coherence in polariton condensates with time-resolved tomography, *Phys. Rev. Lett.* **130**, 113601 (2023).
 - [8] J. C. Bronski, L. D. Carr, B. Deconinck, and J. N. Kutz, Bose-Einstein condensates in standing waves: The cubic nonlinear Schrödinger equation with a periodic potential, *Physical Review Letters* **86**, 1402 (2001).
 - [9] J. M. Dudley, G. Genty, A. Mussot, A. Chabchoub, and F. Dias, Rogue waves and analogies in optics and oceanography, *Nature Reviews Physics* **1**, 675 (2019).
 - [10] J. Bec and K. Khanin, Burgers turbulence, *Physics Reports* **447**, 1 (2007).
 - [11] L. Kofman and A. C. Raga, Analysis of Carleman linearization of lattice Boltzmann, *The Astrophysical Journal* **390**, 359 (1992).
 - [12] C. Xue, Y.-C. Wu, and G.-P. Guo, Quantum homotopy perturbation method for nonlinear dissipative ordinary differential equations, *New Journal of Physics* **23**, 123035 (2021).
 - [13] J.-P. Liu, H. Ø. Kolden, H. K. Krovi, N. F. Loureiro, K. Trivisa, and A. M. Childs, Efficient quantum algorithm for dissipative nonlinear differential equations, *Proceedings of the National Academy of Sciences of the USA* **118**, e2026805118 (2021).
 - [14] W. Itani and S. Succi, Analysis of Carleman linearization of lattice Boltzmann, *Fluids* **7**, 24 (2022).
 - [15] T. Carleman, Application de la théorie des équations intégrales linéaires aux systèmes d'équations différentielles non linéaires, *Acta Mathematica* **59**, 63 (1932).
 - [16] O. Kyriienko, A. E. Paine, and E. Elfving, Solving nonlinear differential equations with differentiable quantum circuits, *Physical Review A* **103**, 052416 (2021).
 - [17] M. Schuld and N. Killoran, Quantum machine learning in feature Hilbert spaces, *Physical Review Letters* **122**, 040504 (2019).
 - [18] M. Lubasch, J. Joo, P. Moinier, M. Kiffner, and D. Jaksch, Variational quantum algorithms for nonlinear problems, *Physical Review A* **101**, 010301 (2020).
 - [19] D. Jaksch, P. Givi, A. J. Daley, and T. Rung, Variational quantum algorithms for computational fluid dynamics, *AIAA Journal* **61**, 1885 (2023).
 - [20] A. J. Pool, A. D. Somoza, C. M. Keever, M. Lubasch, and B. Horstmann, Nonlinear dynamics as a ground-state solution on quantum computers (2024), arXiv:2403.16791

- [quant-ph].
- [21] A. Peruzzo, J. McClean, P. Shadbolt, M.-H. Yung, X.-Q. Zhou, P. J. Love, A. Aspuru-Guzik, and J. L. O'Brien, A variational eigenvalue solver on a photonic quantum processor, *Nature Communications* **5**, 4213 (2014).
- [22] J. Ingelmann, S. Bharadwaj, P. Pfeffer, K. Sreenivasan, and J. Schumacher, Two quantum algorithms for solving the one-dimensional advection-diffusion equation (2024), arXiv:2401.00326 [quant-ph].
- [23] R. Demirdjian, D. Gunlycke, C. A. Reynolds, J. D. Doyle, and S. Tafur, Variational quantum solutions to the advection-diffusion equation for applications in fluid dynamics, *Quantum Information Processing* **21**, 322 (2020).
- [24] F. Y. Leong, W.-B. Ewe, and D. E. Koh, Variational quantum evolution equation solver, *Scientific Reports* **12**, 10817 (2022).
- [25] F. Y. Leong, D. E. Koh, W.-B. Ewe, and J. F. Kong, Variational quantum simulation of partial differential equations: Applications in colloidal transport, *International Journal of Numerical Methods for Heat & Fluid Flow* **33**, 3669 (2023).
- [26] N. M. Guseynov, A. A. Zhukov, W. V. Pogosov, and A. V. Lebedev, Depth analysis of variational quantum algorithms for the heat equation, *Physical Review A* **107**, 052422 (2023).
- [27] Y. Y. Liu, Z. Chen, C. Shu, S. C. Chew, B. C. Khoo, X. Zhao, and Y. D. Cui, Application of a variational hybrid quantum-classical algorithm to heat conduction equation and analysis of time complexity, *Physics of Fluids* **34**, 117121 (2023).
- [28] A. J. Pool, A. D. Somoza, M. Lubasch, and B. Horstmann, Solving partial differential equations using a quantum computer, 2022 IEEE International Conference on Quantum Computing and Engineering , 864 (2022).
- [29] R. H. Byrd, P. Lu, J. Nocedal, and C. Zhu, A limited memory algorithm for bound constrained optimization, *SIAM Journal on Scientific Computing* **16**, 1190 (1995).
- [30] D. Pathria and J. L. Morris, Pseudo-spectral solution of nonlinear schrödinger equations, *Journal of Computational Physics* **87**, 108 (1990).
- [31] L. Fioroni, L. Gravina, J. Stefaniak, A. Baumgärtner, F. Finger, D. Dreon, and T. Donner, A Python GPU-accelerated solver for the Gross-Pitaevskii equation and applications to many-body cavity QED (2024), arXiv:2404.14401 [physics.comp-ph].
- [32] G. Benenti and G. Strini, Quantum simulation of the single-particle Schrödinger equation, *American Journal of Physics* **76**, 657 (2008).
- [33] M. Nielsen and I. Chuang, *Quantum Computation and Quantum Information: 10th Anniversary Edition* (Cambridge University Press, Cambridge, UK, 2010).
- [34] L. Wright, C. M. Keever, J. T. First, R. Johnston, J. Tillay, S. Chaney, M. Rosenkranz, and M. Lubasch, Noisy intermediate-scale quantum simulation of the one-dimensional wave equation (2024), arXiv:2402.19247.
- [35] Qiskit contributors, Qiskit: An open-source framework for quantum computing (2023).
- [36] M. Larocca, N. Ju, D. Garcia-Martin, P. J. Coles, and M. Cerezo, Theory of overparametrization in quantum neural networks, *Nature Computational Science* **3**, 542 (2023).
- [37] R. Shaffer, L. Kocia, and M. Sarovar, Surrogate-based optimization for variational quantum algorithms, *Physical Review A* **107**, 032415 (2023).